Geomechanics and Engineering, *Vol. 29, No. 4 (2022) 471-486*
https://doi.org/10.12989/gae.2022.29.4.471

Numerical analysis of segmental tunnel linings - Use of the beam-spring and solid-interface methods

Alireza Rashiddel[1a], Mohsen Hajihassani[1b], Mehdi Kharghani[2c], Hadi Valizadeh[3d], Reza Rahmannejad[4e] and Daniel Dias*[5,6]

[1]*Department of Mining, Faculty of Engineering, Urmia University, Urmia, Iran*
[2]*Department of Mining, Faculty of Engineering, Islamic Azad University, Science and Research Branch of Tehran, Iran*
[3]*Civil Engineering Department, Özyeğin University, 34794 Çekmeköy, Istanbul, Turkey*
[4]*Department of Mining, Faculty of Engineering, Shahid Bahonar University, Kerman, Iran*
[5]*Department of Civil Engineering, Grenoble Alps University, Laboratory 3SR, Polytech Grenoble, France*
[6]*Geotechnical Expert, Antea Group, Antony, France*

(Received August 9, 2021, Revised April 9, 2022, Accepted April 16, 2022)

Abstract. The effect of segmental joints is one of main importance for the segmental lining design when tunnels are excavated by a mechanized process. In this paper, segmental tunnel linings are analyzed by two numerical methods, namely the Beam-Spring Method (BSM) and the Solid-Interface Method (SIM). For this purpose, the Tehran Subway Line 6 Tunnel is considered to be the reference case. Comprehensive 2D numerical simulations are performed considering the soil's calibrated plastic hardening model (PH). Also, an advanced 3D numerical model was used to obtain the stress relaxation value. The SIM numerical model is conducted to calculate the average rotational stiffness of the longitudinal joints considering the joints bending moment distribution and joints openings. Then, based on the BSM, a sensitivity analysis was performed to investigate the influence of the ground rigidity, depth to diameter ratios, slippage between the segment and ground, segment thickness, number of segments and pattern of joints. The findings indicate that when the longitudinal joints are flexible, the soil-segment interaction effect is significant. The joint rotational stiffness effect becomes remarkable with increasing the segment thickness, segment number, and tunnel depth. The pattern of longitudinal joints, in addition to the joint stiffness ratio and number of segments, also depends on the placement of longitudinal joints of the key segment in the tunnel crown (similar to patterns B and B').

Keywords: beam-spring; joint position; rotational stiffness; segment thickness; soil-segment; solid-interface

1. Introduction

In recent years, mechanized shield tunneling is being used increasingly for tunnel excavation in urban areas owing to reduce buildings damage and excavation time (Lee *et al.* 2001, Ding *et al.* 2004, Do *et al.* 2013, Golpasand *et al.* 2018, Yu *et al.* 2019, Wang *et al.* 2019, Rezaei *et al.* 2019, Xue *et al.* 2019, Liu *et al.* 2020, Rashiddel *et al.* 2020, Ramesh *et al.* 2020, Ramsheh *et al.* 2021). Due to the high cost of prefabricated segmental lining in shielded tunneling projects, further studies are necessary to design and understand the segmental tunnel lining behavior accurately. As shown in Fig. 1(a), segments of a ring are linked by segmental joints (longitudinal joints) and ring by ring joints (circumferential joints) (Blom 2002, Koyama 2003, Hefny and Chua 2006, Huang *et al.* 2006, Zaheri *et al.* 2020). The segmental lining is generally designed as a continuous lining, while this assumption is a conservative simplification of the natural tunnel structure behavior because the lining bending moment increases (Wood 1975, Lee and Ge 2001). According to Fig. 1(b), the transmission of structural forces and stress distribution differs regarding the low flexural stiffness of longitudinal joints compared to a continuous lining (ITA 2000). As a result, the segmental joint's stiffness and geometry strongly influenced the deformations and structural forces in the segmental tunnel (Wood 1975, JSCE 2016). Therefore, the segmental lining behavior is significantly affected by the joints and connections stiffness (Do *et al.* 2013). Recent field observations and laboratory research have also revealed that leakages can be attributed to the lining joint deformations (opening, offset, rotation). This is relevant when the sealing performance of the segmental joints is also taken into account. The tunnel lining behavior is composed of structural and sealant behavior (Gong *et al.* 2020).

In recent decades, many researchers have attempted to simulate the segment joints and investigate their effects on

*Corresponding author, Professor
E-mail: Daniel.dias@univ-Grenoble-Alpes.fr
[a]M.Sc
E-mail: st_a.rashiddel@urmia.ac.ir
[b]Ph.D.
E-mail: m.hajihassani@urmia.ac.ir
[c]Ph.D.
E-mail: kharghani.m@gmail.com
[d]Ph.D.
E-mail: hadi.valizadeh@ozu.edu.tr
[e]Ph.D.
E-mail: sreza99@uk.ac.ir

ISSN: 2005-307X (Print), 2092-6219 (Online)

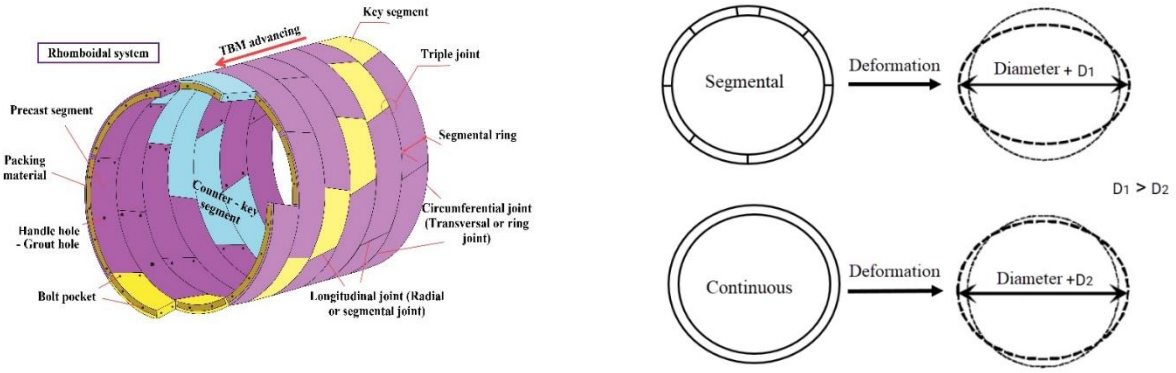

(a) Staggered configuration of joints with other details

(b) Deformability of segmental lining versus continuous lining

Fig. 1 Segmental tunnel structure

the behavior of structures by analytical and numerical methods (Lee *et al.* 2001, Blom 2002, Koyama 2003, Ding *et al.* 2004, Hefny and Chua 2006, Huang *et al.* 2006, Luttikholt 2007, El Naggar and Hinchberger 2008, Arnau and Molins 2011, Do *et al.* 2013, Kavvadas *et al.* 2017, Nematollahi *et al.* 2018, Rashiddel *et al.* 2020). In general, direct and indirect methods are utilized to consider the segmental and ring joints. The tunnel structure is supposed as a rigid ring without segment joints in an indirect approach. The impact of the joints is then considered through a reduction coefficient of the bending rigidity. Among the limitations of this method the incapability to consider the geometry and configuration of joints could be mentioned. In contrast, the joints are considered directly in the lining in the direct method. The influence of segmental joints through the indirect method was considered by Wood (1975). An empirical equation was proposed using the effective moment of inertia method to calculate the reduction coefficient of the bending rigidity, as in Eq. (1). Furthermore, using laboratory tests, the Japanese Society of Civil Engineers (JSCE 2016) indirectly considered the segmental joint bending rigidity. A reduction factor of the bending rigidity (η) between 20% and 40% and a transfer coefficient of the bending moment (ζ) between 30% and 50% are used to take into account the segmental joints (Koyama 2003, Guglielmetti *et al.* 2007, Teachavorasinskun and Chub-Uppakarn 2010, Yu *et al.* 2019). No equations were provided to calculate the bending moment transmission coefficient (ζ) amount under lining configuration and buried condition (Liu *et al*. 2022).

$$I_e = I_j + \left(\frac{4}{n}\right)^2 I \qquad (I_e \le I, n > 4) \tag{1}$$

where I_j is the moment of inertia in the joint location, I is the tunnel lining moment of inertia, and n is the number of joints in the lining.

Numerical methods were used simultaneously with other methods to analyze the segmental tunnel lining behavior. In this regard, two general approaches were developed. The first approach (ground-spring model) deals with the tunnel structure modeling, and the ground loads are transferred to the lining through separate springs (Blom 2002, Klappers *et al.* 2006, Oreste 2007, Do *et al.* 2013, Chaipanna and Jongpradist 2019). In the second approach (geotechnical model), the tunnel lining's structural behavior and the surrounding ground are considered (Do *et al.* 2013). Using the Finite Element Method (FEM), Hefny and Chua (2006) simulated a 6 m diameter tunnel segmental lining. The number of segments and joint patterns has significantly impacted the maximum bending moment. Using the FEM, Teachavorasinskun and Chub-Uppakarn (2010) investigated the bending moment distribution on a segmental lining. The obtained results showed that the rotational stiffness of segmental joints ranges from 1 to 3 MN.m/rad/m. Arnau and Molins (2011) analyzed a segmental tunnel lining using a full-scale in-situ model and FEM software in two and three dimensions. Based on their results, the rotational stiffness of the segmental joints is estimated between 40 to 80 MN.m/rad/m. Do *et al.* (2013) simulated the segmental tunnel structure using the FDM (Finite Difference Method). The numerical results showed that the number of joints greatly impacts the overall bending moment when the coefficient of lateral earth pressure is lower or higher than unity ($K_0 \neq 1$). In comparison with rotational stiffness, Axial and radial stiffness has a negligible impact on the action of the segmental tunnel structure. Similarly, Guan *et al.* (2015) simulated the segmental tunnel lining using FDM. They found that the effective ratio of bending rigidity increased intensely by improving the soil properties. An advanced three-dimensional numerical simulation of the shield-driven tunneling method was developed by Kavvadas *et al.* (2017) using FEM. They assumed the rotational stiffness of segmental joints equal to 230 MN.m/rad/m. They showed a significant increase in the lining rigidity due to staggering joints, which were close to the stiffness of a continuous one. In the study of Nematollahi *et al.* (2018), the segmental joints were simulated with an oblique angle to the tunnel axis and compared with segmental lining results with straight joints. It has permitted us to show the importance of accurate modeling of the segmental joint geometry. Ebrahimi *et al.* (2020) simulated the opening construction influence in the segmental lining using a 3D finite element simulation. Their model considered the interaction between longitudinal joints using a friction coefficient and solid elements.

Segmental joint behavior was represented using the stiffness characteristics of the joint connection using rotational, axial, and radial springs (Do *et al.* 2013, Kavvadas *et al.* 2017, Nematollahi *et al.* 2018). Researchers

used various values for segmental joint rotational stiffness, but the accuracy of these values was not evaluated. Multiple methods are available to measure segmental joint rotational stiffness. Janssen (1983) proposed a simple theoretical model to describe the bending moment behavior of segmental joints. These joints were modeled by an equivalent concrete beam between two adjacent segments. However, Janssen's theoretical model cannot account for the extra joint rotation in the elastic phase for thin longitudinal joints. According to the applied assumptions in this model, the longitudinal joints were considered closed in the elastic phase of the real condition. This assumption can only be used for a thick segmental lining (Luttikholt 2007). Van Der Vliet (2006) performed a two-dimensional finite element analysis of joints under normal load and bending moment for comparison with Janssen's (1983) and Gladwell's (1980) analytical methods. He found the theoretical relation of Gladwell (1980) in good agreement with the numerical method of the finite element. Nevertheless, analytical methods for calculating the joint rotational stiffness have limitations.

Due to the limitations of the above methods, this paper used a new method, SIM, to calculate and extract the rotational stiffness of longitudinal joints. This method eliminates the cost of using large-scale tests to determine rotational stiffness. In the SIM method, the rotational stiffness of each segmental lining longitudinal joint is evaluated. The rotational stiffness of the joints is also determined under positive and negative bending moments.

In this paper, the segmented structure of the Tehran Subway is studied in two and three dimensions using BSM and SIM approaches. A new model is presented in this research to analyze the segmented tunnel structure action (SIM). The body and longitudinal joints of the segments are simulated using components of the solid and interface elements, respectively. Accurately, the SIM model calculates the rotational stiffness of the segmental joints. This parameter is then used to carry out a comprehensive parametric analysis in the BSM models.

2. BSM and SIM numerical methods

The segmental tunnel lining analysis methods can be divided into several categories by Lee *et al.* (2001), Koyama (2003), Huang *et al.* (2006), and JSCE (2016), including a ring with uniform flexural rigidity (no joints), Multi-Hinged ring and Beam-Spring model. The simplest way to simulate tunnel lining is to use a beam element (Luttikholt 2007). In the Beam-Spring method, the segmental tunnel lining is assumed as rings with rotational and shear springs. Moreover, segments are simulated as straight or curved beams while the longitudinal and circumferential joints are respectively considered using rotational and shear springs. If the rotational stiffness in the Beam-Spring model is set equal to zero, it becomes a Multiple Hinged joints model. In the case of assuming infinity for stiffness, it converts to the no joints method. The Beam-Spring model is suitable to investigate the bending rigidity reduction and the effect of segmental joints as a staggering pattern (Huang *et al.* 2006, JSCE 2016).

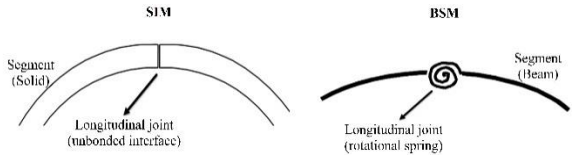

(a) SIM and BSM model in this paper

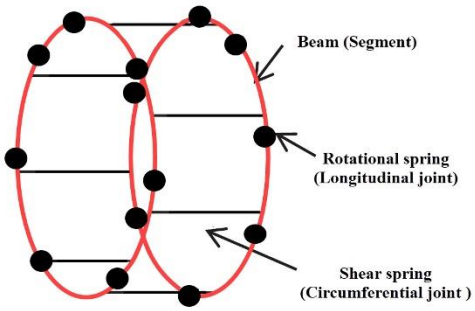

(b) Known model for the Beam-Spring method

Fig. 2 Schematic view of the longitudinal joints modeling

Calculation of the rotational stiffness in segmental joints is essential in this method and depends on various factors. This paper uses the SIM model as a new method to calculate the longitudinal joint's rotational stiffness. Fig. 2 shows a schematic description of the BSM and SIM models versus the well-known Beam-Spring method.

Although solid elements are more precise than beam and shell elements, they have a higher calculation time due to their geometric complexity (Yanzhi *et al.* 2014). Despite this disadvantage, due to the exact element shape generation, the joint rotational stiffness does not have to be computed to simulate the segmental joint behavior, which is a significant advantage. Obtaining the joint rotational stiffness requires full-scale in-situ tests, which are costly and time-consuming. Considering a non-linear rotational stiffness of segmental joints is another advantage of the SIM approach. Regarding the real segmental joints shape in the SIM model, joints exposed to a positive bending moment will show more stiffness than joints subjected to a negative one (Lee *et al.* 2001, Andreotti *et al.* 2020). According to Lee *et al.* (2001), the longitudinal joint's rotational stiffness with a positive bending moment is 2 or 3 times greater than the longitudinal joints with a negative bending moment. The connection between segment-segment and soil-segment is considered by setting an interface element. This element can simulate a normal and shear interaction between two materials in contact. The parameters related to the interface elements are chosen according to their mode of functioning (Itasca 2016):

1. An interface harder than the material around, allowing a slip and probably opening (interface between segment-segment).
2. An interface soft enough to affect the system's performance (interface between soil-segment).

3. Case study

A cross-section of the Tehran Subway Line 6 Tunnel was selected as a reference case. Line 6 begins from the

southeast and ends in the northwest of the city, the longest and most popular tunnel route in Tehran. In the initial plan, 27 stations were built over 30 km. As the city expands, a growth plan of four additional stations (27+4 stations) for 10 km (30+10 km) has been considered. According to Fig. 3, a schematic shape is shown from the transverse section of the Line 6 Tunnel. It includes two layers, sandy clay (L1), clayey sand, and clayey gravel (L2) (BHSL-612). This transverse section was selected as the reference for the numerical simulations regarding the soil height, water table, soil strength parameters, and the longitudinal geological profile.

3.1 Soil model and calibration of soil rigidities

The selection of appropriate constitutive models for soils is important for the tunneling process's numerical modeling and, consequently, the correct prediction of the lining pressures. Considering that a constant stiffness would not be an appropriate approximation for a detailed study of surface settlements for all shear strain levels (Hejazi *et al.* 2008). Shear and volumetric hardening are the constituent plastic hardening model for the soil behavior simulation. The model is characterized by the hyperbolic stress-straining relationship in drained axial compression (while unloading/reloading is elastic) and stress dependency defined by a power law. It also includes shear and volumetric hardening regulations and the Mohr-Coulomb failure criterion. Also, the soil compressibility is explained by three non-linear rigidities concerning the stress levels ($E_{50}^{ref} - E_{oed}^{ref} - E_{ur}^{ref}$). The first numerical modeling step is the soil mechanical parameters calibration using the on-site monitoring data. At this stage, soil rigidity parameters are calibrated using the settlement monitoring data.

Using surveying equipment, monitoring allowed to collect data. Indicator pins were used to track surface settlements. These pins were installed above the tunnel centerline, parallel to the tunnel path. Fig. 4 displays the surface settlements collected for the reference case. According to this figure, the surface settlements were monitored at five points above the ground. The maximum surface settlement derived from the monitoring data equals 36 mm. As mentioned, rigidity parameters for the soil layers ($E_{50}^{ref} - E_{oed}^{ref} - E_{ur}^{ref}$) are calibrated using the surface settlement monitoring results. Table 1 displays all the soil characteristics for the considered cross-section.

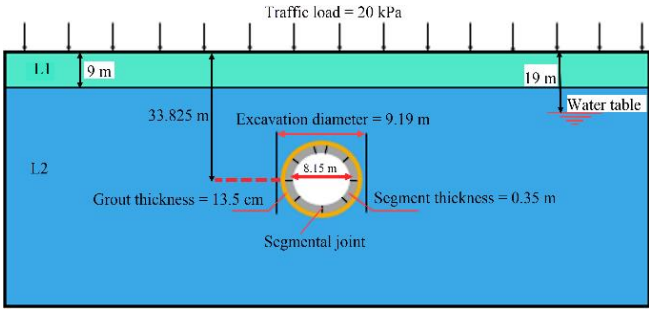

Fig. 3 Selected cross-section (reference case)

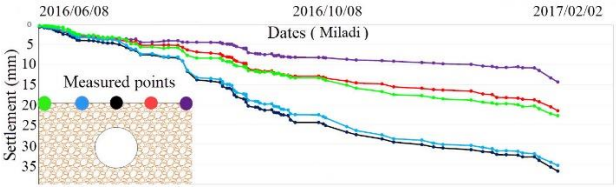

Fig. 4 Cumulative surface settlements at the monitored section

Table 1 Hardening Soil properties for the ground layers (Darya Khak Pey Consulting Engineers 2009)

Parameters	Symbol	Values	Values	Unit
Soil stratum	L	L_1(CL)	L_2(SC-GC)	-
Range	h	0-9	9-68	m
Dry density	ρ_{dry}	1710	1700	Kg/m^3
Saturated density	ρ_{sat}	2100	2100	Kg/m^3
Young's Modulus	E	15	100	MPa
Secant Young's Modulus	E_{50}^{ref}	20	133	MPa
Unloading-reloading Young's Modulus	E_{ur}^{ref}	60	400	MPa
Oedometric Young's Modulus	E_{oed}^{ref}	16	106.5	MPa
Poisson's ratio	ν	0.4	0.35	-
Poisson's ratio of PH model	ν_{PH}	0.2	0.2	-
Cohesion	C	35	30	kPa
Friction angle	ϕ°	28	30	Degree
In-situ stress ratio	K_0	0.5	0.65	-
K_0-value for normal consolidation	K_0^{nc}	0.53	0.5	-
A janbu-type parameter	m	0.5	0.5	-
Failure ratio	R_f	0.9	0.9	-
Reference pressure	P^{ref}	100	100	kPa

3.2 Mechanical and geometrical parameters of the segmental lining

Each concrete ring is formed by two trapezoidal, one key, and six rectangular segments. Each prefabricated concrete ring's width is equal to 1.5 m with a 0.35 m thickness, and the outer diameter is equal to 8.85 m. The shape of the entire ring can be found in Fig. 5(a). In Fig. 5(b), the longitudinal joints are equipped with grooves for the guiding rods and the circumferential joint is plain. Adjacent rings are connected with dowels (GMBH Consulting Engineers 2011). To simulate the segmental structure, a linear-elastic model is used. Table 2 displays the mechanical and geometrical features of the tunnel structure used on Tehran Subway Line 6. The characteristics of the shield EPB-TBM (Earth Pressure Balance-Tunnel Boring Machine) are shown in Table 3.

Table 2 Concrete ring characteristics in Tehran Subway Line 6 (GMBH Consulting Engineers 2011)

Width of the lining ring	Outer diameter of the ring	Segment effective thickness	Segment thickness	Uniaxial compressive strength	Poisson's ratio	Young's Modulus	Unit weight
l (mm)	D (mm)	t_e (mm)	t (mm)	f_c (MPa)	v	E (GPa)	γ (kN/m^3)
1500	8850	245	350	35	0.2	27.8	25

Table 3 Shield parameters in Tehran Subway Line 6 (Herrenknecht 2009)

Cutter head (Excavation diameter)	Tail skin (diameter)	Front shield (diameter)	Length of the shield	Shield thickness	Poisson's ratio	Young's Modulus	Unit weight
D (mm)	D (mm)	D (mm)	l (mm)	t (mm)	v	E (GPa)	γ (kN/m^3)
9190	9120	9150	9250	100	0.3	210	78.50

4. Numerical simulation of the segmental lining

4.1 Three-dimensional model (calculate stress relaxation)

The tunnel face's three-dimensional effect should be considered if the tunnel is analyzed in 2D plain strain conditions. The displacement of the tunnel crown starts from the unexcavated section and increases as it approaches the tunnel face. All of these deformations are related to the third dimension parallel to the tunnel's axis. In a two-dimensional model, it should be considered using a stress relaxation parameter. The three-dimensional building tunnels process is established in 2D models using a stress relaxation coefficient (λ_d) and the Convergence - Confinement method (CV-CF) (Eq. (2)). The pressure reduction on the tunnel wall enables the effect of the forward tunnel breast to be simulated.

$$\sigma = (1 - \lambda_d)\sigma_0 \tag{2}$$

where σ is the pressure at the tunnel crust (kPa), σ_0 is the in-situ stress in the ground (kPa), and λ_d is the stress relaxation coefficient.

Given that our reference case is in reality excavated and supported, we do not look at tunnel lining modeling and design as an original design, so it is not possible to use the GRC curve to determine the optimal stress relaxation coefficient (because the design TBM, shield, tunnel lining, and grout injection were already done). Two methods are then possible. The first method is to use the settlement monitoring results. The second method uses an advanced three-dimensional model by considering the conical shield and over-excavation. Because monitoring data were used to calibrate the soil rigidity in 2D models, it is impossible to use monitoring data simultaneously to find the stress relaxation coefficient. Therefore, according to the field conditions, a three-dimensional model is used.

According to Fig. 6, the three-dimensional numerical model was considered and can model the following processes, including grout injection, segmental lining, and conical shield, to find the stress relaxation coefficient of the two-dimensional model. Nematollahi and Dias (2019)

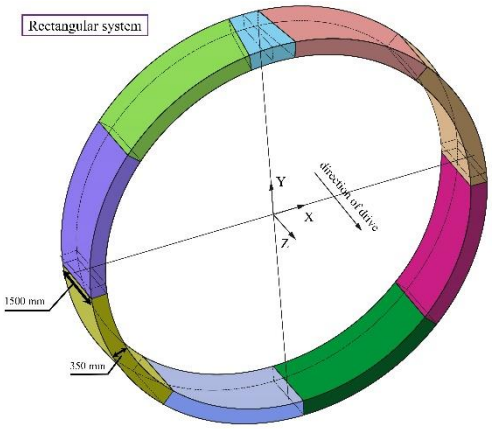

(a) Assembled segments

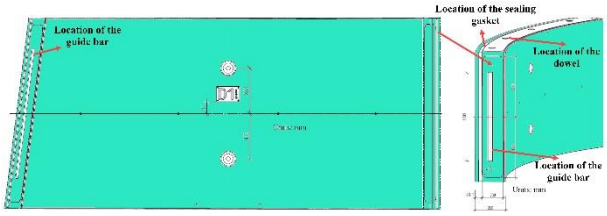

(b) Details of the segment

Fig. 5 Three-dimensional view of the segmental tunnel structure

method was used to simulate the conical of the TBM shield. The shell element was used to model the conical shield and also the liner element was used to model the segments and the segmental and ring joints were modeled using the link element with 6 degrees of freedom. The rotational stiffness of the segmental joints was calculated using the SIM method presented in the following sections. According to the equation of the Dutch Centre Underground Bowen (COB), face pressure in the three-dimensional numerical model was obtained (Guglielmetti *et al.* 2007). The amount of face pressure is 281.5 kPa with a gradient of 12.7 kPa.

Fig. 7 shows the vertical and horizontal displacement contours in the 3D model of the tunnel. According to Fig. 7(a), the maximum surface settlement is about 33 mm and it differs 3 mm from the surface settlement monitoring results.

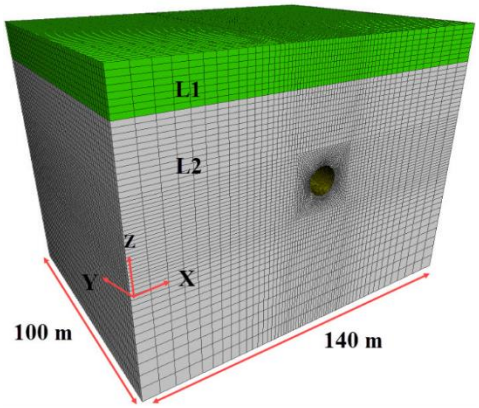

(a) Geometry and meshing

(b) Configuration of joints and segments

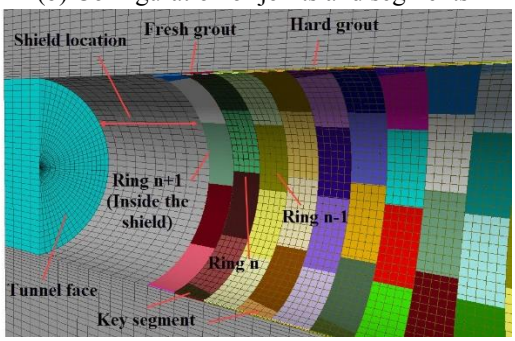

(c) Details of 3D numerical model

Fig. 6 Three-dimensional numerical model

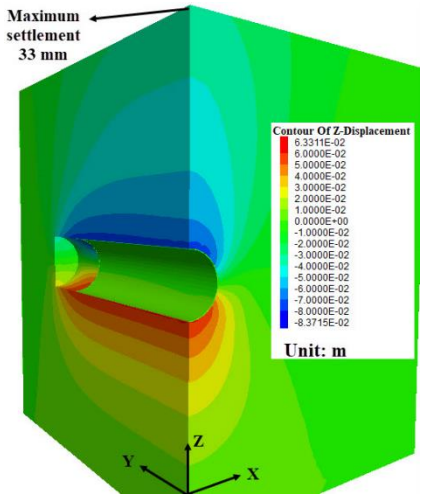

(a) Vertical displacement

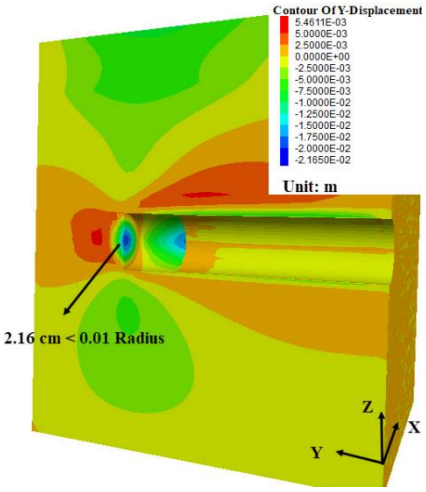

(b) Horizontal displacement

Fig. 7 Displacement contours of 3D model

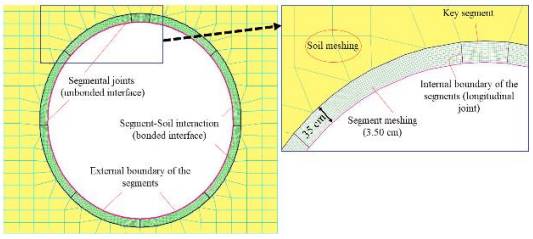

Fig. 8 SIM model with interfaces, soil meshing, and segment meshing

This low difference indicates the accuracy of advanced 3D modeling of mechanized tunnels. Also, the Mohr-Coulomb constitutive model (MC) for soil is used in the 3D model. The high displacement of the tunnel invert is due to the MC model in Fig. 7(a). According to Fig. 7(b), the maximum displacement of the tunnel face is about 2.16 cm and it is less than one-hundredth of the tunnel radius. Finally, the tunnel face is stable. According to this 3D numerical model, the stress relaxation coefficient due to the third dimension was obtained equal to 0.6 and used in the SIM and BSM models.

4.2 Two-dimensional model (SIM model)

The actual thickness and rectangular section of the concrete lining can be numerically simulated using solid elements (Rashiddel *et al.* 2020). Thus, this part simulates the segmental tunnel structure using solid components, whereas interface components establish the connection and rotation of the segmental joints. The model shown in Fig. 8 indicates the segmental structure selected SIM. According to this figure, the mesh size of the segment used in the SIM is 3.5 cm. The total length of the numerical model is 140 m and its height is 68 m. These geometry and mesh sizes were selected according to a sensitivity analysis. The lower boundary is fixed horizontally and vertically. The lateral boundaries are fixed horizontally. According to this figure,

Table 4 Interface properties for the segment-segment interaction (SIM model) (Rashiddel *et al*. 2020)

Parameter	Symbol	Value
Normal stiffness coefficient (Pa/m)	K_N	8.8×10^{12}
Shear stiffness coefficient (Pa/m)	K_S	8.8×10^{12}
Cohesion (Pa)	C	0.0
Dilation angle (°)	ψ	0.0
Friction angle (°)	φ	35.0
Tensile bond strength (Pa)	T	0.0
Shear bond strength ratio	S	100

Table 5 Interface properties for the soil-segment interaction (SIM and BSM models) (Rashiddel *et al*. 2020)

Parameter	Symbol	Value
Radial rigidity coefficient (Pa/m)	K_r	1.72×10^{8}
Tangential rigidity coefficient (Pa/m)	K_t	5.73×10^{7}
Cohesion (Pa)	C	20×10^{3}
Dilation angle (°)	ψ	0.0
Friction angle (°)	φ	17.0
Tensile bond strength (Pa)	T	6.7×10^{4}
Shear bond strength ratio	S	100

nine unbonded interfaces are located on the longitudinal joint thickness. The slide and separation behavior of segmental joints must be modeled on the unbonded interface (zero tensile bond strength). Table 4 provides the properties for the interface components of the segmental joints. The interaction between segments and soil is also built with a bonded interface feature in Fig. 8. Table 5 presents the properties used for soil-segment interface components.

For slipped and separated interfaces, their normal and shear stiffness can be calculated using the equivalent stiffness of surrounding material, like the interface at the contact of the segmental joints. In Table 4, the longitudinal joint's normal and shear stiffness are determined using a rule of thumb approximately ten times the stiffest adjacent zone's equivalent stiffness by Eq. (3) (Itasca 2016). In contrast, interfaces between segment and soil must use actual values of the normal and shear rigidities (for softer interfaces than the surrounding materials). In Table 5, the radial spring rigidity (K_r) on the interface soil-segment with Eq. (4) was determined using Winkler's hypothesis, which matches the closed-form solution of the elastic ground circular tunnel.

Also, in the equation suggested by Plizzari and Tiberti (2006), the tangential spring rigidity (K_t) was also considered by using Eq. (5) (Molins and Arnau 2011).

$$\text{ES (Equivalent Stiffness)} = max\left[\frac{\left(K+\frac{4}{3}G\right)}{\Delta z_{min}}\right] \tag{3}$$

where K and G are the bulk and shear modulus, respectively, and Δz_{min} is the smallest dimension of the neighboring zone in the normal direction.

$$K_r = \frac{E_s}{R(1+\nu)} \tag{4}$$

$$K_t = \frac{K_r}{3} \tag{5}$$

where E_s is the Young's Modulus of soil (Pa), R is the external lining radius (m), and ν is the soil Poisson's ratio.

4.3 Two-dimensional model (BSM model)

In the selected cross-section, the stress relaxation coefficient to be considered equal to 0.6 to obtain a 3 cm displacement at the excavation crown (for Phase 2). This is achievable on the in-situ ground as the TBM has 4 cm of overcutting in diameter and 3 cm because of its conical shield in diameter. A sensitivity analysis was conducted to eschew the impact of boundaries on results. The overall length of the BSM is 140 meters, and the height of the numerical model is 68 meters, as indicated in Fig. 9.

The number of elements used for the beam structural elements is equal to 408 elements and the largest grout mesh size is 7 cm. Drained conditions have been used for the BSM and SIM models because of the high soil permeability (10^{-5} m/s). Under these conditions, drained soil parameters are used. The soil-segment interface components in the BSM and SIM models shall be subject to the parameters used in Table 5.

4.4 Tunneling process in 2D models

The numerical stages of shield tunneling are simulated based on the field stages:

- **Phase 0 (Initial State)**: The material properties were allocated after geometry and mesh generation. Then the initial conditions for boundary conditions and stresses were also determined. In the end, the model hits an initial balance.
- **Phase 1 (Initial State)**: When a surface charge of 20 kPa is applied because of the traffic load at the upper border, the model achieves a balance status.
- **Phase 2 (shield installation)**: The first point is the initialization of deformations due to the former balance. The tunnel is excavated, the TBM shield is mounted, and the model is solved.
- **Phase 3 (stress relaxation)**: Next, a 0.6 stress relaxation coefficient ($0.3 \leq \lambda_d \leq 0.7$) is used to remove the shield. The relaxation coefficient value is obtained from 3D advanced numerical simulations. The BSM and SIM models used the same relaxation value.
- **Phase 4 (segment installation and tail void grouting)**: After installation of the solid grout for a thickness of 13.5 cm and the segmental ring, considering maximum stress relaxation factor (λ_d=1), in the excavated ground area and on the segmented structure is applied the grout injection pressure (normal pressure).
- **Phase 5 (grout hardening)**: At this point, the grout injection pressure was removed, and the consolidated grout parameters (1-day grout properties) were taken into account.

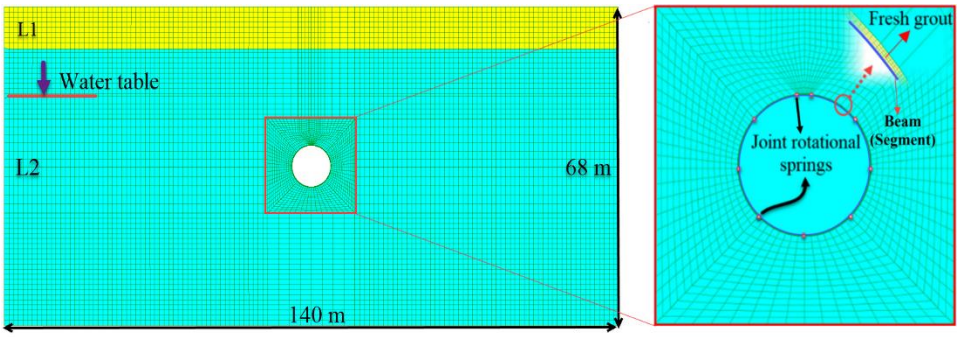

(a) Geometry and meshing

(b) Rotational spring's position, segment, and fresh grout

Fig. 9 BSM model

• **Phase 6 (grout hardening)**: The parameters of the 28-day grout properties are taken into account at this point

4.5 Results in terms of settlements

As shown in Fig. 10, both the BSM and SIM models have been studied with settlement monitoring results in Fig. 4 to calibrate the secant Young's Modulus using measured surface settlement curves. Therefore, there is a strong agreement between the numerical and monitoring outcomes in the maximum settlement. The impact of tunnel face on settlement in 2D models should be mentioned by using the 2D axial symmetry numerical model, according to Ramesh *et al.* (2020) added. According to Fig. 10, the difference in the settlement curve in the left-hand area is related to surcharges such as buildings with different weights on the right tunnel side or the presence of a greenfield area on the left tunnel side (Stiros and Kontogianni 2009, Kontogianni and Stiros 2020). Due to lack of data, in numerical modeling, a uniform constant load is considered at the ground surface.

4.6 Rotational stiffness efforts

The Solid-Interface model has a certain bending moment distribution, Because SIM models the real segment thickness and interface. The SIM model gives the fixed bending moment in the joint's location. It was then divided to the rotational opening of the joints, $K_\theta=M/\theta$ (based on the bending moment created at the joint's positions and the amount of joints opening). The average values of the joint's rotational stiffness in the SIM model were obtained with a mathematical method to assign the average values of the rotational stiffness of the joints in the BSM. Ultimately, the rotational stiffness captured is 118 MN.m/rad/m. This amount is similar to Koyama (2003) and Do *et al.* (2013) results. The plastic moment capacity in the longitudinal joint of the Beam-Spring model was calculated by Eq. (6) (Itasca 2016, Rashiddel *et al.* 2020).

$$M_p = \sigma_y \left[\frac{bh^2}{4}\right] \quad (6)$$

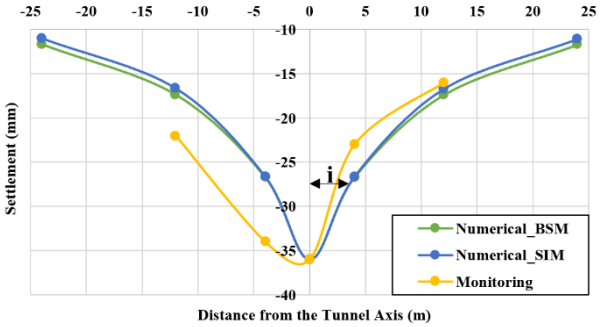

Fig. 10 Surface settlement troughs obtained by the BSM, SIM models, and monitoring data

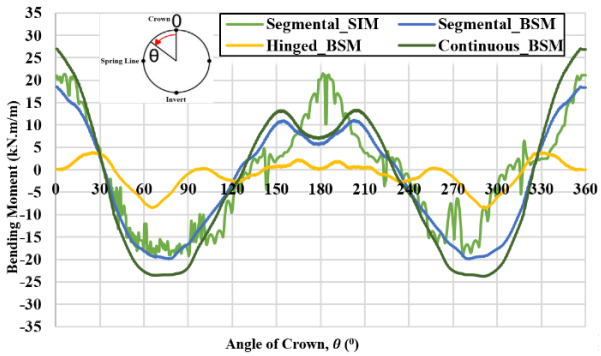

Fig. 11 Distribution of bending moment in tunnel lining

where M_p is the plastic moment, b and h are the width and effective thickness of the segment, respectively, and σ_y is the yield stress of the segment section.

In Fig. 11, both the SIM and BSM models are presented with bending moment distributions. The small difference between the segmental BSM and SIM models on the invert of the tunnel (θ=180) is for reason the segment joint's high stiffness at a positive bending moment. In the continuous structure for the BSM model, the maximum bending moment is the same as 27.1 kN.m/m. The values of the maximum bending moment in the segmental models of the SIM and BSM are 20.1 and 18.1 kN.m/m, respectively. The lower bending moment in the Hinged-BSM simulations is supposed to be the tunnel structure with hinged joints. As shown in Fig. 11, the longitudinal joints of the segmental structure can be subjected to positive and negative bending

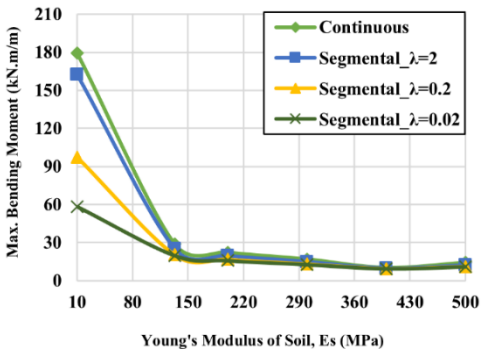

(a) Maximum bending moment

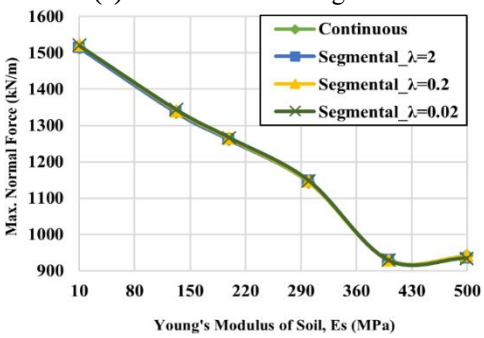

(b) Maximum normal force

Fig. 12 Variation of the maximum internal forces in the tunnel lining with the soil Young's Modulus

moments, therefore, exhibit different behavior. This different behavior is due to the loading conditions. The BSM model is an equivalent method and considers the same stiffness for the longitudinal joint springs. Due to the complexity of the segment geometry modeling in the SIM model and its expensive calculation time, using it only to obtain the longitudinal joint's rotational stiffness is recommended. Consequently, the BSM model is used for parametric analysis in this study.

5. Parametric Analysis by the BSM model

A parametric analysis was conducted to comprehensively explore the segmental tunnel lining behavior for different conditions. All parametric analysis used the reference case data and the following items:

- The surrounding ground of the tunnel is considered homogeneous and completely dry.
- The stress relaxation of the surrounding tunnel ground is not considered to accept the worst situation for the tunnel structure's internal forces.
- The Plastic Hardening constitutive model is used for the ground in one layer (L_2 (SC-GC)).

In order to present the relationship between the internal structural forces and displacement for different joint stiffness, a dimensionless parameter called the joint stiffness ratio ($\lambda=K_\theta l/EI$) to describe the relative joint stiffness is added over the segment body stiffness (Lee *et al.* 2001, Naggar and Hinchberger 2008). The calculation length l is usually taken equal to 1 m to represent a typical unit length. The parameter EI is the bending rigidity of continuous tunnel support.

5.1 Influence of ground Young's Modulus (E_S)

A Young's Modulus in the range between 10 to 500 MPa is considered for the following parametric analysis. It permits an investigation of Young's Modulus values for soft soils to soft rocks. For a comprehensive study, joint stiffness ratios equal to 0.02, 0.2, and 2 are used. A no-slip mode between the structure and the surrounding ground is considered. The distribution of the maximum bending moment along the tunnel structure versus Young's Modulus is illustrated in Fig. 12(a). This figure shows that the lining segmentation effect on the bending moment is insignificant for Young's Modulus higher than 150 MPa. In other words, the tunnel lining segmentation effect on the bending moment is more remarkable for soft soils. By increasing the segmental joint flexibility, the maximum bending moment is significantly reduced. This result is similar to Do *et al.* (2013) and Hefny and Chua (2006). Fig. 12(b) shows the maximum normal force in the tunnel lining for various Young's Modulus. According to this figure, the segmental lining does not affect the normal force in the lining. The same behavior is seen by increasing the elastic modulus for the continuous and segmental linings considering different joint stiffness ratios.

5.2. Influence of the ground-segment interaction

According to in-situ tests, Molins and Arnau (2011) found that considering a perfect tangential rigidity ($K_t = \frac{K_r}{3}$) between the lining and soil in numerical modeling would provide the best fitting results with in-situ outputs. The decrease in tangential rigidity reduced the maximum axial stress, a smoothing distribution, and an increase of the stresses induced at the invert lining zone. Because of this, the slippage plays a vital role in the ground-segment interaction, especially in complex ground conditions. According to the previous studies, sliding at the ground-segment interface is only probable for tunnels constructed in very soft soils, in cases where the seismic loading intensity is high, and when the grout is at a liquid state. Therefore, the ground-segment interaction should be investigated for three modes: no-slip, full-slip, and real state condition (between no-slip and full-slip modes). The full and no-slip modes are modeled on the interaction between the segments and the ground around the tunnel as follows (Sedarat *et al.* 2009):

A) In the direction normal to the segment, ground and segment are entirely connected.

B) Full-slip and no-slip modes are modeled in the tangential direction on the tunnel lining. There is a complete tangential adhesion between the ground and the tunnel lining in the no-slip state. As a result, a glued interface with normal and shear rigidity coefficients (equivalent to attach) is used at the ground-structure interface (According to Eq. (3)). While in a full-slip state, no friction is considered between the ground and lining structure, and the tangential resistance is zero. A bonded interface element with a certain normal rigidity coefficient is used to simulate a complete

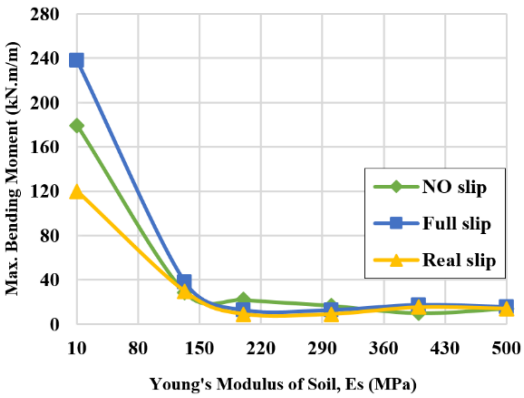

(a) Continuous lining

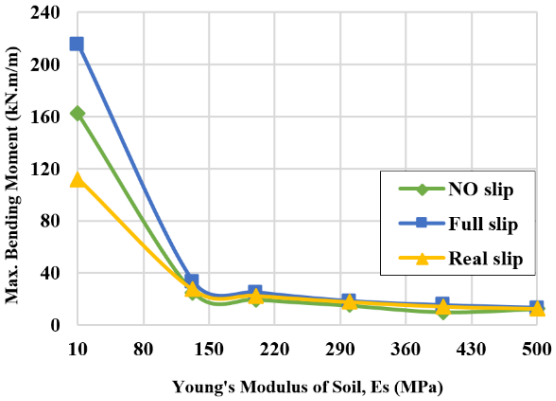

(b) Segmental lining with λ equal 2

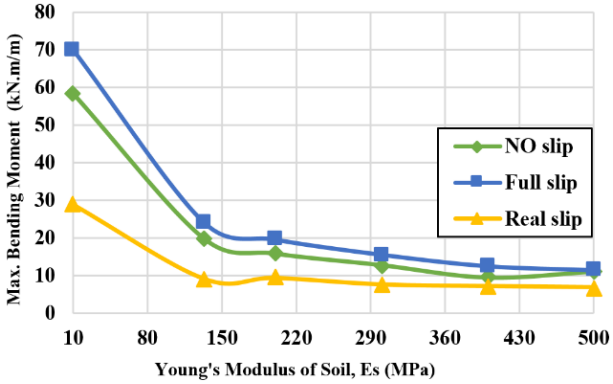

(c) Segmental lining with λ equal 0.02

Fig. 13 Variation of the maximum bending moment in the tunnel lining for various Young's Modulus and various structure-ground conditions

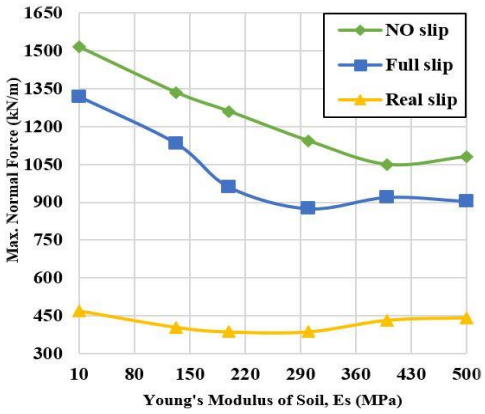

(a) Continuous lining

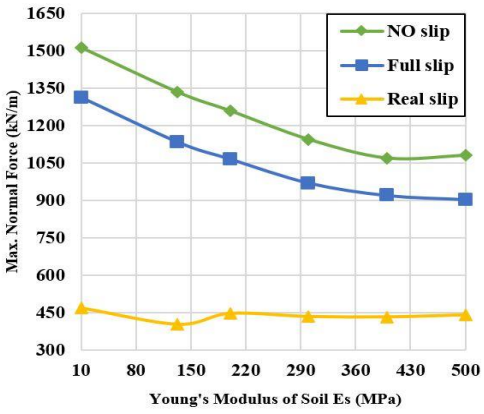

(b) Segmental lining with λ equal 2

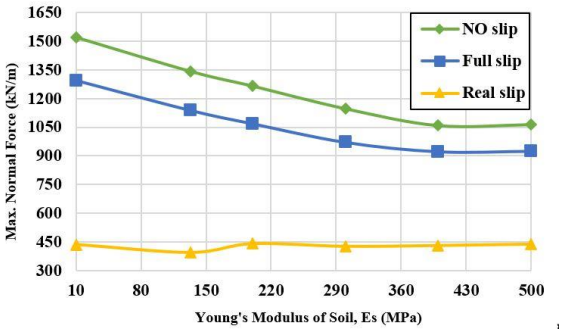

(c) Segmental lining with λ equal 0.02

Fig. 14 Variation of the maximum normal force in the lining for various Young's Modulus and various structure-ground conditions

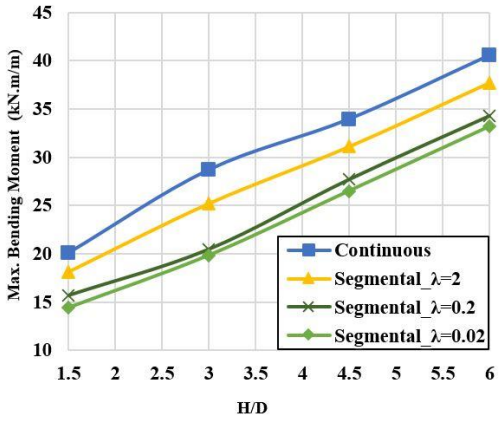

(a) Maximum bending moment (PH constitutive model)

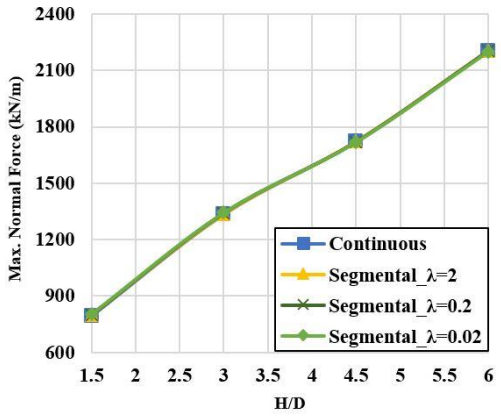

(b) Maximum normal force (PH constitutive model)

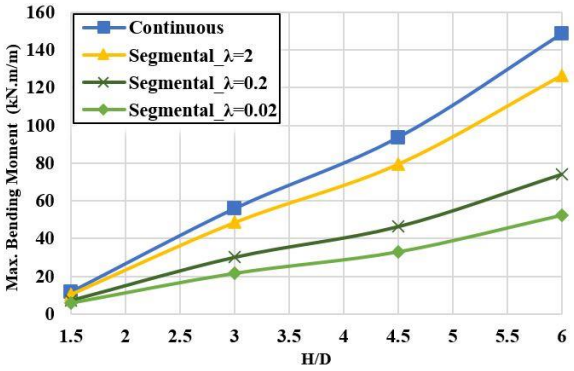

(c) Maximum bending moment (MC constitutive model)

Fig. 15 Variation of the maximum structural internal forces versus depth to diameter ratios

full-slip condition (Eq. (3)), and a nominal tangential rigidity coefficient equal to 1000 Pa/m is used. Moreover, the normal and tangential rigidity coefficients for real slip conditions were determined by Winkler's hypothesis (Eqs. (4) and (5)).

Fig. 13(a) displays the maximum bending moment distribution induced in the continuous lining for different ground Young's Modulus. According to this figure, for Young's Modulus above 150 MPa, ground-structure interaction conditions do not affect the caused maximum bending moment in the lining. In addition, for values lower than 150 MPa under real slip conditions, the lowest maximum bending moment was observed. The increase of the Young's Modulus reduces the overall bending moment in the lining. The maximum bending moment caused in the segmental structure with a λ equal to 2 versus Young's Modulus is shown in Fig. 13(b). According to this figure, for Young's Modulus above 150 MPa, different interaction conditions do not affect the induced maximum bending moment. Also, the lowest maximum bending moment was observed for values lower than 150 MPa under real slip conditions. The maximum bending moment caused in the segmental structure with λ equal to 0.02 versus Young's Modulus is shown in Fig. 13(c). According to this figure, the different interaction conditions affect the maximum bending moment for all Young's Modulus. Using the real soil-structure interaction is important and induces a noticeable decrease in the maximum bending moment.

According to the results presented in Figs. 13, it can be seen that in soft soils, the soil-structure interaction has a significant effect on the tunnel lining bending moment.

The normal force distribution caused in the continuous and segmental structures (λ equal 0.02 and 2) for different Young's Modulus is presented in Figs. 14(a)-14(c). Regarding these figures, the normal forces decrease by increasing the Young's Modulus for both continuous lining and segmental lining (no-slip and full-slip conditions). In real-slip conditions for all Young's Modulus values, increasing the Young's Modulus has no effect on the induced normal forces for the continuous and segmental lining. Consequently, from Figs. 13 and 14, it can be concluded that the real-slip condition permits an optimum design definition. The no-slip and full-slip conditions will induce an overestimated design. Finally, the real-slip conditions between the lining and surrounding ground are necessary for accurate design.

5.3 Influence of the tunnel depth (H)

In general, the depth of metro tunnels from the ground surface to the tunnel crown is 1.5 to 6 times the tunnel diameter. High depths will cause higher stress levels and higher costs. Low depths will lead to the possibility of instabilities at the tunnel crown and significant surface settlements. Depth to diameter ratios (*H/D*) of 1.5, 3, 4.5, and 6 are used to investigate the tunnel depth effect on

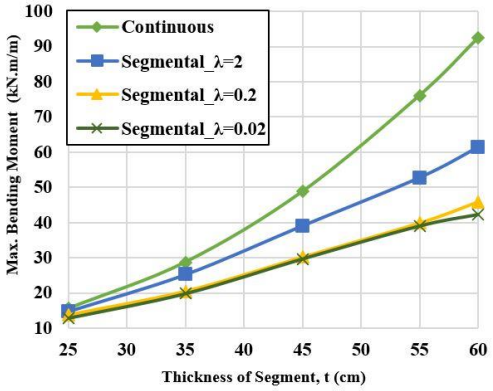

(a) Maximum bending moment

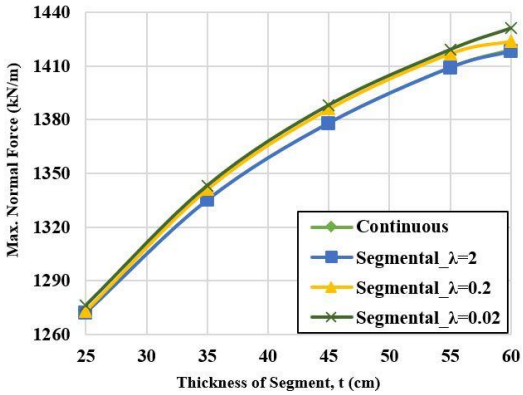

(b) Maximum normal force

Fig. 16 Variation of maximum structural internal forces versus lining thickness

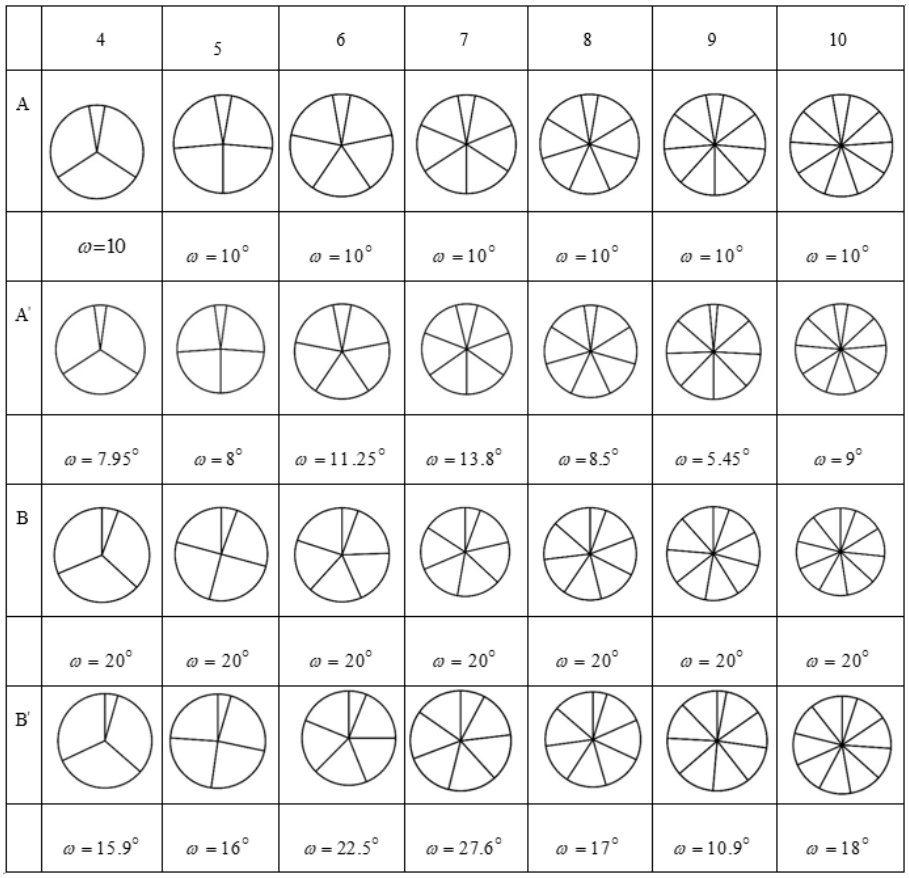

Fig. 17 Segmental joint patterns with a number of 4 to 10 segments

segmental lining internal forces. For this purpose, the joint stiffness ratios are considered in the scope from 0.02 to 2. Fig. 15(a) indicates the maximum bending moment of the tunnel structure versus the depth to diameter ratios (with the PH constitutive model). This figure shows that the lining segmentation does not affect the maximum bending moment when considering the tunnel overburden. The induced maximum normal forces in the tunnel lining versus the tunnel overburden are presented in Fig. 15(b). As can be seen in this figure, tunnel segmentation does not affect the maximum normal force. Increasing the tunnel depth increases the maximum normal forces for the segmental and continuous structure.

Fig. 15(c) displays the effects of the lining segmentation on the maximum bending moment when increasing the tunnel overburden in the Mohr-Coulomb constitutive model (MC constitutive model). In the continuous lining, the overall bending moment is higher than in the segmented lining. In tunnels with stiffer joints, the effect of the lining segmentation is lower and induces an increase in bending moment with an increase in the tunnel depth. According to this figure, a segmental lining with more flexible joints

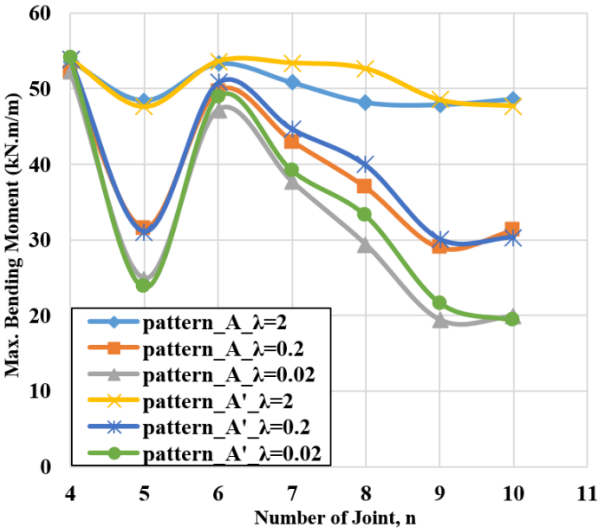

(a) Patterns A and A'

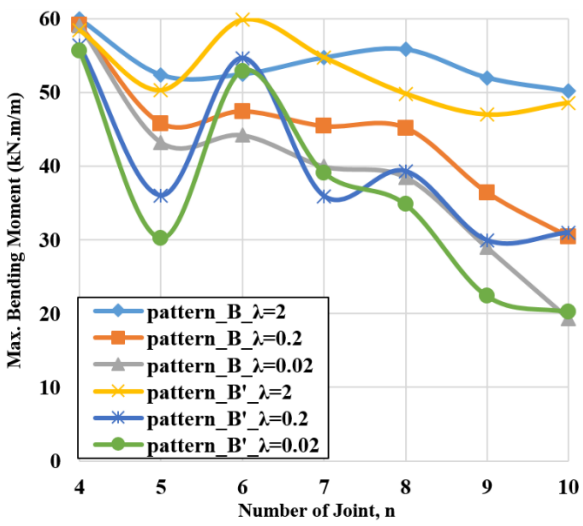

(b) Patterns B and B'

Fig. 18 Variation of the maximum bending moment for different segment numbers and different patterns

significantly affects the bending moment drop with the tunnel depth increase. Fig. 15(c) findings agree well with Hefny and Chua (2006) results. The reason for investigating the tunnel depth effect on the segmental lining behavior with the Mohr-Coulomb constitutive model is related to Hefny and Chua (2006) results. In Fig. 15(a), the plastic hardening constitutive model is used and it gives different results from Hefny and Chua (2006). It shows the necessity of using advanced constitutive models to evaluate the behavior of segmental tunnel linings more accurately.

5.4 Influence of the segment thickness (t)

The tunnel lining thickness depends on the applied loads on the lining (ground and water pressure), dynamic loads (storage, transportation, and segment installation), and waterproofing requirements (sealing cushion). In general, a tunnel lining with a 25 to 60 cm thickness is used (Vigle 2001). In this research, the segment thickness is studied in this range (25 to 60 cm).

As the tunnel lining thickness increases, the weight of the support and the tunnel lining rigidity increase. As a result, overall normal forces and the bending moment of the segmental tunnel lining also increase. The maximum bending moment in the tunnel lining concerning the lining thickness is presented in Fig. 16(a). By increasing the lining thickness, the maximum bending moment increases. This increase is higher for continuous structure. For the segmental structure case with flexible joints, the impact of increasing its thickness is lower, and the graph tends to have a constant value. For a lining thickness of 25 cm, the segmentation effect on the bending moment is negligible. Consequently, the maximum bending moment in the continuous and the segmental lining is similar. This is due to the reduced rigidity of the lining as the thickness becomes thinner. Fig. 16(b) shows the variation of the maximum normal forces in the lining to the segment thickness. Increasing the lining thickness from 25 to 60 cm gradually increases the maximum normal forces in a similar way for the continuous and segmental lining. The findings are well endorsed by Hefny and Chua (2006) on the segmental tunnel joints. However, Hefny and Chua (2006) used a tunnel lining flexibility ratio (F) instead of the lining thickness parameter.

5.5 Influence of the longitudinal joint patterns and the number of segments (n)

As shown in Fig. 1, the segmental joints are installed in a staggered position. This method increases the segmental lining's overall rigidity and is more resistant to sealing and the TBM jacking thrusts (German Tunneling Committee (DAUB) 2001). During the installation of segmental joints, the behavior of joints against the bending moments is crucial. The longitudinal joint position and geometry should then be considered for an optimal design (JSCE 2016). This part investigates the effect of longitudinal joint patterns and the number of segments (n). Hefny and Chua (2006), Naggar and Hinchberger (2008), Teachavorasinskun and Chub-Uppakarn (2010), and Do *et al.* (2013) have studied the number of segments and joint patterns. However, in all these studies, the key segment was ignored. In reality, a smaller segment called "key segment" is used to complete the segmental ring. In this study, four different segmental joint patterns with key segments joint near the tunnel crown (A, A′) and at the crown (B, B′) were used (see Fig. 17). Patterns A' and B' with various segment numbers were selected from various projects (Yanzhi *et al.* 2014, Li *et al.* 2015, Zheng *et al.* 2017, Zhang *et al.* 2019, Gong *et al.* 2020, Wang *et al.* 2019). Therefore, the key segment size is variable. The tunnel's diameter is assumed to be constant and equal to 8.85 m. An in-situ stress ratio of 0.65 is applied in all models. The angle between the tunnel crown and the key segment joints is introduced as a joint reference angle (ω) by measuring it from the tunnel crown in the clockwise direction. Fig. 18 shows the studied segmental joint patterns considering a number of 4 to 10 segments. Fig. 18(a) shows that the maximum induced bending moment decreases by

increasing the segment numbers in A and A' patterns. In high rigid joints ($\lambda = 2$), the maximum bending moment is less reduced when the number of segments increases. In Fig. 18(a), the bending moment curves are drastically reduced for a number of five segments. With five segments, the segmental joints position in both patterns is in positions with high bending moments. As a result, these joint positions induce a noticeable decrease in the overall bending moment. In contrast, a higher number of segments does not always mean lower bending moments, whereas the longitudinal joint pattern plays a vital role. Furthermore, the effect of the longitudinal joint patterns decreases by increasing the segment number. So, for a segmental lining with joint patterns B and B', the bending moment diagram is similar to the one of patterns A and A' (Fig. 18(b)). When considering a number of segments equal to five, the maximum bending moment reduction in the B pattern joints is lower than for the other patterns. This is because the joints are in areas with a lower bending moment (Fig. 18(b)). With regards to Figs. 18(a) and 18(b), the maximum bending moment reduction in various joint patterns is related to the longitudinal joint location and the bending moment distribution around the tunnel structure. Finally, the maximum bending moment is approximately equal by reducing the segment numbers (n=4) for all patterns. This result is in good agreement with Eq. (1).

6. Conclusions

This paper used BSM and SIM approaches to investigate the segmental tunnel structure behavior. Using the SIM model, the average rotational stiffness of the longitudinal joint was calculated to be used in the BSM model. The rotational stiffness of longitudinal joints was calculated considering the bending moment distribution of joints and opening of joints in the SIM model. Then the BSM model is used for parametric analysis. The results can be resumed as follows:

• In previous studies, specific patterns were proposed without a key segment for longitudinal joint positions. However, these joint patterns are not realistic if a key segment tunnel is used. Finally, it can be said that the longitudinal joint position can be more effective if there are longitudinal joints in positions where a lot of structural loads are applied. The load distribution on the tunnel structure depends on the in-situ stress ratio and the static and dynamic loads. In addition to the ratio of joint stiffness and number of segments, the pattern of longitudinal joints also depends on the longitudinal joint's placement of the key segment at the tunnel crown. If the key segment joints are not located exactly at the tunnel crown, the longitudinal joint pattern effect in the segmental tunnel lining design is lost.

• The Elastic-Plastic behavior of the tunnel lining segmental joints depends on the loading conditions and the appropriate constitutive soil model (PH model). A SIM model is suggested to achieve joint rotational stiffness values due to the real condition of the joints and segments.

• Increasing the segment number induces a decrease in the maximum bending moment. However, the longitudinal joint pattern strongly influences the bending moment in a tunnel structure with a few segments. As the number of segments increases, the effect of the longitudinal joint patterns is extremely reduced.

• In a segmental lining relative to the continuous lining, when increasing the tunnel overburden, the bending moment does not increase considerably. The joint rotational stiffness (Kro) influence is more significant when increasing the tunnel depth.

• There is no significant increase in the tunnel internal forces in a segmental structure with a low joint stiffness ratio (λ) as the segment thickness increases. The effect of joint rotational stiffness on the bending moment becomes more significant by increasing the segment's thickness.

• The interaction conditions affect the normal force on the tunnel lining and the bending moment, especially for tunneling in soils. However, by reducing the stiffness of segmental joints, the impact of soil-structure interaction is visible even on hard grounds.

• The joint stiffness ratio (λ) plays a crucial role in designing the segmental lining. The influence of the soil-segment interaction conditions is more remarkable when the joint stiffness ratio is lower.

• For grounds with Young's Modulus of more than 150 MPa, the lining segmentation impact is eliminated, and the behavior of segmental and continuous linings is similar.

References

Andreotti, G., Calvi, G.M., Soga, K., Gong, C. and Ding, W. (2020), "Cyclic model with damage assessment of longitudinal joints in segmental tunnel linings", *Tunn. Undergr. Sp. Tech.*, **103**, 103472. https://doi.org/10.1016/j.tust.2020.103472.

Arnau, O. and Molins, C. (2011), "Experimental and analytical study of the structural response of segmental tunnel linings based on an in situ loading test. Part 2: Numerical simulation", *Tunn. Undergr. Sp. Tech.*, **26**(6), 778-788. https://doi.org/10.1016/j.tust.2011.04.005.

Blom, C. (2002), "Design philosophy of concrete linings for tunnel in soft soils", Ph.D. Dissertation, Delft University of Technology (TU Delft), Delft.

Chaipanna, P. and Jongpradist, P. (2019), "3D response analysis of a shield tunnel segmental lining during construction and a parametric study using the ground-spring model", *Tunn. Undergr. Sp. Tech.*, **90**, 369-382. https://doi.org/10.1016/j.tust.2019.05.015.

Darya Khak Pey Consulting Engineers (2009), "Geotechnical studies report the southern part of the metro Tehran line 6", Tehran Urben Railway Corporation.

Ding, W.Q., Yue, Z.Q., Tham, L.G., Zhu, H.H., Lee, C.F. and Hashimoto, T. (2004), "Analysis of shield tunnel", *Int. J. Numer. Anal. Method. Geomech.*, **28**(1), 57-91. https://doi.org/10.1002/nag.327.

Do, N.A., Dias, D., Oreste, P. and Djeran-Maigre, I. (2013), "2D numerical investigation of segmental tunnel lining behavior", *Tunn. Undergr. Sp. Tech.*, **37**, 115-127. https://doi.org/10.1016/j.tust.2013.03.008.

Ebrahimi, S., Hadei, M.R. and Rashiddel, A. (2020), "Numerical investigation of innovative support frame of openings in the segmental tunnel lining", *Open Constr. Build. Technol. J.,* **14**, 358-369. https://doi.org/10.2174/1874836802014010358.

El Naggar, H. and Hinchberger, S.D. (2008), "An analytical solution for jointed tunnel linings in elastic soil or rock", *Can. Geotech. J.*, **45**(11), 1572-1593. https://doi.org/10.1139/T08-075.

German Tunneling Committee (DAUB) (2001), "Concrete Lining for Tunnel Built by Underground Construction", German Committee for Underground Construction.

Gladwell, G.M. (1980), *Contact Problems in the Classical Theory of Elasticity*, Springer Science & Business Media.

GMBH Consulting Engineers (2011), "Report on the static design of the segmental lining for MetroTehran Line 6", Tehran Urben Railway Corporation.

Golpasand, M.R.B., Do, N.A., Dias, D. and Nikudel, M.R. (2018), "Effect of the lateral earth pressure coefficient on settlements during mechanized tunneling", *Geomech. Eng.*, **16**(6), 643-654. https://doi.org/10.12989/gae.2018.16.6.643.

Gong, C., Ding, W. and Xie, D. (2020), "Parametric investigation on the sealant behavior of tunnel segmental joints under water pressurization", *Tunn. Undergr. Sp. Tech.*, **97**, 103231. https://doi.org/10.1016/j.tust.2019.103231.

Guan, Z., Deng, T., Wang, G. and Jiang, Y. (2015), "Studies on the key parameters in segmental lining design", *J. Rock Mech. Geotech. Eng.*, **7**(6), 674-683. https://doi.org/10.1016/j.jrmge.2015.08.008.

Guglielmetti, V., Grasso, P., Mahtab, A. and Xu, S. (2007), *Mechanized Tunnelling in Urban Areas: Design Methodology and Construction Control*, Taylor & Francis Group, London, UK.

Hefny, A.M. and Chua, H.C. (2006), "An investigation into the behaviour of jointed tunnel lining", *Tunn. Undergr. Sp. Tech.*, **21**(3), 428. https://doi.org/10.1016/j.tust.2005.12.070.

Hejazi, Y., Dias, D. and Kastner, R. (2008), "Impact of constitutive models on the numerical analysis of underground constructions", *Acta Geotech.*, **3**(4), 251-258. https://doi.org/10.1007/s11440-008-0056-1.

Herrenknecht A.G. (2009), "S-523 Earth Pressure Balance Shield", Tehran Metro Line 3.

Huang, Z.r., Zhu, W., Liang, J.h., Lin, J. and Jia, R. (2006), "Three-dimensional numerical modelling of shield tunnel lining", *Tunn. Undergr. Sp. Tech.*, **21**(3), 434. https://doi.org/10.1016/j.tust.2005.12.076.

Working Group No. 2, International Tunnelling Association (ITA) (2000), "Guidelines for design of shield tunnel lining", *Tunn. Undergr. Sp. Tech.*, **15**(3), 303-331. https://doi.org/10.1016/S0886-7798(00)00058-4.

Itasca Consulting Group Inc. (2019), *FLAC-Fast Lagrangian Analysis of Continua (Version 8.1)*, Minneapolis, Minnesota, User′s manual.

Itasca Consulting Group Inc. (2012), *FLAC3D-Fast Lagrangian Analysis of Continua* (Version 5.0), Minneapolis, Minnesota, User′s manual.

Janssen, p. (1983), "Tragverhalten von Tunnelausbauten mit Gelenktübbings [Load carrying behavior of segmented tunnel linings]", Technische Universitat Carolo-Wilhelmina zu Braunschweig, Braunschweig (In German).

JSCE (2016), *Standard Specifications for Tunnelling: Shield Tunnels*, Working Group for Shield Tunnels, Tokyo.

Kavvadas, M., Litsas, D., Vazaios, I. and Fortsakis, P. (2017), "Development of a 3D finite element model for shield EPB tunnelling", *Tunn. Undergr. Sp. Tech.*, **65**, 22-34. https://doi.org/10.1016/j.tust.2017.02.001.

Klappers, C., Grübl, F. and Ostermeier, B. (2006), "Structural analyses of segmental lining – coupled beam and spring analyses versus 3D-FEM calculations with shell elements", *Tunn. Undergr. Sp. Tech.*, **21**(3), 254-255. https://doi.org/10.1016/j.tust.2005.12.116.

Kontogianni, V. and Stiros, S.C. (2020), "Ground loss and static soil–structure interaction during urban tunnel excavation: evidence from the excavation of the athens metro", *Infrastructures,* **5**(8). https://doi:10.3390/infrastructures5080064.

Koyama, Y. (2003), "Present status and technology of shield tunneling method in Japan", *Tunn. Undergr. Sp. Tech.*, **18**(2), 145-159. https://doi.org/10.1016/S0886-7798(03)00040-3.

Lee, K.M., Hou, X.Y., Ge, X.W. and Tang, Y. (2001), "An analytical solution for a jointed shield-driven tunnel lining", *Int. J. Numer. Anal. Methods Geomech.*, **25**(4), 365-390. https://doi.org/10.1002/nag.134.

Li, X., Yan, Z., Wang, Z. and Zhu, H. (2015), "A progressive model to simulate the full mechanical behavior of concrete segmental lining longitudinal joints", *Eng. Struct.*, **93**, 97-113. https://doi.org/10.1016/j.engstruct.2015.03.011.

Liu, B., Yu, Z., Han, Y., Wang, Z., Yang, S. and Liu, H. (2020), "A simplified combined analytical method for evaluating the effect of deep surface excavations on the shield metro tunnels", *Geomech. Eng.*, **23**(5), 405-418. https://doi.org/10.12989/gae.2020.23.5.405.

Liu, X., Zhang, Y., Bao, Y. and Song, W. (2022), "Investigation of the structural effect induced by stagger joints in segmental tunnel linings: Numerical explanation via macro-level structural modeling", *Tunn. Undergr. Sp. Tech.*, **120**, 104284. https://doi.org/10.1016/j.tust.2021.104284.

Luttikholt, A. (2007), "Ultimate limit state analysis of a segmented tunnel lining - Results of Full-scale Tests Compared to Finite Element Analysis", Master thesis, Delft University of Technology (TU Delft), Delft.

Molins, C. and Arnau, O. (2011), "Experimental and analytical study of the structural response of segmental tunnel linings based on an in situ loading test: Part 1: Test configuration and execution", *Tunn. Undergr. Sp. Tech.*, **26**(6), 764-777. https://doi.org/10.1016/j.tust.2011.05.002.

Nematollahi, M., Molladavoodi, H. and Dias, D. (2018), "Three-dimensional numerical simulation of the Shiraz subway second line-influence of the segmental joints geometry and of the lagging distance between twin tunnels' faces", *Eur. J. Environ. Civ. Eng.*, **24**(10), 1606-1622. https://doi.org/10.1080/19648189.2018.1476270.

Nematollahi, M. and Dias, D. (2019), "Three-dimensional numerical simulation of pile-twin tunnels interaction – Case of the Shiraz subway line", *Tunn. Undergr. Sp. Tech.*, **86**, 75-88. https://doi.org/10.1016/j.tust.2018.12.002.

Ramesh, A., Hajihassani, M. and Rashiddel, A. (2020), "Ground movements prediction in shield-driven tunnels using gene expression programming", *Open Constr. Build. Technol. J.*, **14**, 286-297. https://doi.org/10.2174/1874836802014010286.

Ramsheh, F.A., Rashiddel, A. and Dias, D. (2021), "3D numerical simulations of tunneling induced soil deformations", *J. Phys. Conference Series*, **1973**(1), 012207. https://doi:10.1088/1742-6596/1973/1/012207.

Rashiddel, A., Kharghani, M., Dias, D. and Hajihassani, M. (2020), "Numerical study of the segmental tunnel lining behavior under a surface explosion – Impact of the longitudinal joints shape", *Comput. Geotech.,* **128**, 103822. https://doi.org/10.1016/j.compgeo.2020.103822.

Rezaei, A.H., Shirzehhagh, M. and Golpasand, M.R.B. (2019), "EPB tunneling in cohesionless soils: A study on Tabriz Metro settlements", *Geomech. Eng.*, **19**(2), 153-165. https://doi.org/10.12989/gae.2019.19.2.153.

Sedarat, H., Kozak, A., Hashash, Y.M.A., Shamsabadi, A. and Krimotat, A. (2009), "Contact interface in seismic analysis of circular tunnels", *Tunn. Undergr. Sp. Tech.*, **24**(4), 482-490. https://doi.org/10.1016/j.tust.2008.11.002.

Stiros, S. and Kontogianni, V. (2009), "Mean deformation tensor

and mean deformation ellipse of an excavated tunnel section", *Int. J. Rock Mech. Min. Sci.*, **46**(8), 1306-1314. https://doi.org/10.1016/j.ijrmms.2009.02.013.

Plizzari, G.A. and Tiberti, G. (2006), "Steel fibers as reinforcement for precast tunnel segments", *Tunn. Undergr. Sp. Tech.*, **21**(3), 438-439. https://doi.org/10.1016/j.tust.2005.12.079.

Teachavorasinskun, S. and Chub-uppakarn, T. (2010), "Influence of segmental joints on tunnel lining", *Tunn. Undergr. Sp. Tech*., **25**(4), 490-494. https://doi.org/10.1016/j.tust.2010.02.003.

Vigle, L. (2001), "Design, Manufacturing and Application of Tunnel Segments", International Training course, Sargans, Switzerland.

Van der Vliet, C. (2006), "Langsvoeggedrag op basis van de elasticiteitstheorie, Een aanscherping van de janssen-relatie", Bouwdienst Rijkswaterstaat.

Wang, F.Y., Zhou, M.L., Zhang, D.M., Huang, H.W. and Chapman, D. (2019), "Random evolution of multiple cracks and associated mechanical behaviors of segmental tunnel linings using a multiscale modeling method", *Tunn. Undergr. Sp. Tech*., **90**, 220-230. https://doi.org/10.1016/j.tust.2019.05.008.

Wood, A.M. (1975), "The circular tunnel in elastic ground", *Geotechnique*, **25**(1), 115-127. https://doi.org/10.1680/geot.1975.25.1.115.

Xue, Y., Li, X., Qiu, D., Ma, X., Kong, F., Qu, C. and Zhao, Y. (2019), "Stability evaluation for the excavation face of shield tunnel across the Yangtze River by multi-factor analysis", *Geomech. Eng.*, **19**(3), 283-293. http://doi.org/10.12989/gae.2019.19.3.283.

Yanzhi, Y., Weiwei, Z., Jianwei, W. and Zhihao, Y. (2014), "Three-dimensional orthotropic equivalent modelling method of large-scale circular jointed lining", *Tunn. Undergr. Spa. Tech*., **44**, 33-41. https://doi.org/10.1016/j.tust.2014.07.002.

Yu, H., Cai, C., Bobet, A., Zhao, X. and Yuan, Y. (2019), "Analytical solution for longitudinal bending stiffness of shield tunnels", *Tunn. Undergr. Spa. Tech*., **83**, 27-34. https://doi.org/10.1016/j.tust.2018.09.011.

Zaheri, M., Ranjbarnia, M. and Dias, D. (2020), "3D numerical investigation of segmental tunnels performance crossing a dip-slip fault", *Geomech. Eng.*, **23**(4), 351-364. https://doi.org/10.12989/gae.2020.23.4.351.

Zhang, J.L., Schlappal, T., Yuan, Y., Mang, H.A. and Pichler, B. (2019), "The influence of interfacial joints on the structural behavior of segmental tunnel rings subjected to ground pressure", *Tunn. Undergr. Sp. Tech*., **84**, 538-556. https://doi.org/10.1016/j.tust.2018.08.025.

Zheng, G., Cui, T., Cheng, X., Diao, Y., Zhang, T., Sun, J. and Ge, L. (2017), "Study of the collapse mechanism of shield tunnels due to the failure of segments in sandy ground", *Eng. Fail. Anal.,* **79**, 464-490. https://doi.org/10.1016/j.engfailanal.2017.04.030.

CC